Catal Lett
DOI 10.1007/s10562-017-2192-4

Photochemical Preparation of Anatase Titania Supported Gold Catalyst for Ethanol Synthesis from CO_2 Hydrogenation

Dong Wang[1,2,3,4] · Qingyuan Bi[1] · Guoheng Yin[1] · Peng Wang[1] · Fuqiang Huang[1,3,5] · Xiaoming Xie[2,3] · Mianheng Jiang[2,3]

Received: 22 May 2017 / Accepted: 15 September 2017

Abstract Hydrogenation of the greenhouse gas CO_2 to higher alcohols through catalysis holds great promise for resource transformation in low-carbon energy supply system, but the efficient and selective synthesis of value-added ethanol by a robust heterogeneous catalyst under relatively mild conditions remains a major challenge. Based on our previous work on Au/TiO_2 as an active and selective catalyst for ethanol synthesis, we report here that a facile photochemical route can be used for the preparation of anatase TiO_2 supported gold catalyst (Au/a-TiO_2) for efficient hydrogenation of CO_2. Compared with the conventional deposition-precipitation method requiring strong brønsted base and flammable H_2 gas in the complicated and time-consuming process, the photochemical way for the facile preparation of supported gold catalyst shows the advantages of green and energy-saving. Of significant importance is that an impressive space-time-yield of 869.3 mmol g_{Au}^{-1} h^{-1}, high selectivity, and excellent stability can be readily attained at 200 °C and total pressure of 6 MPa. The effects of irradiation time, solvent, and metal loading or Au particle size on ethanol synthesis are systematically investigated.

Electronic supplementary material The online version of this article (doi:10.1007/s10562-017-2192-4) contains supplementary material, which is available to authorized users.

✉ Qingyuan Bi
biqingyuan@mail.sic.ac.cn

✉ Fuqiang Huang
huangfq@mail.sic.ac.cn

1 State Key Laboratory of High Performance Ceramics and Superfine Microstructure, Shanghai Institute of Ceramics, Chinese Academy of Sciences, Shanghai 200050, People's Republic of China

2 State Key Laboratory of Functional Materials for Informatics, Shanghai Institute of Microsystem and Information Technology, Chinese Academy of Sciences, Shanghai 200050, People's Republic of China

3 School of Physical Science and Technology, ShanghaiTech University, Shanghai 200031, People's Republic of China

4 University of Chinese Academy of Sciences, Beijing 100049, People's Republic of China

5 Beijing National Laboratory for Molecular Sciences and State Key Laboratory of Rare Earth Materials Chemistry and Applications, College of Chemistry and Molecular Engineering, Peking University, Beijing 100871, People's Republic of China

Published online: 14 October 2017

Graphical Abstract

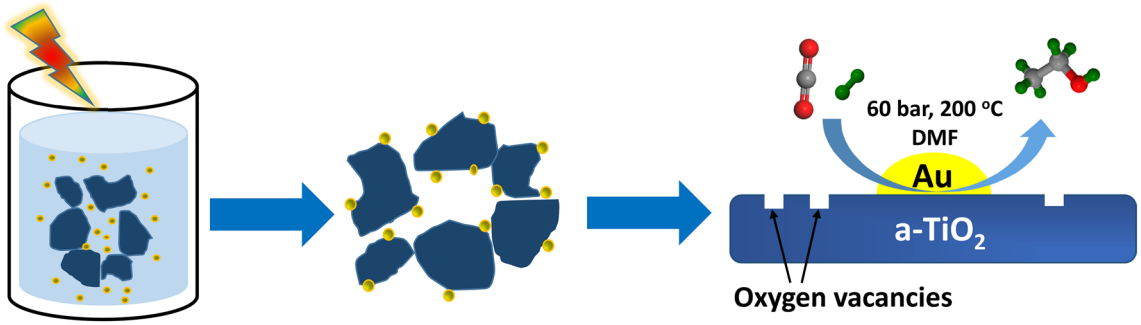

Keywords Gold catalysis · Photochemical route · Anatase titania · Ethanol · CO_2 hydrogenation

1 Introduction

Carbon dioxide (CO_2), an abundant greenhouse gas, has been largely used to produce valuable chemicals and fuels, including methane, formic acid, and alcohols [1–4]. The hydrogenation of CO_2 to yield value-added alcohols (especially methanol and ethanol) as one of the most important means for CO_2 conversion has been attracted ever-increasing attentions [5–7]. Compared with methanol, ethanol (EtOH) and other higher alcohols (HAs) possess higher energy density and show broader applications in fuel additives, neat fuels, and raw chemical materials [8, 9]. However, the thermodynamic stability and chemical inertness of CO_2 molecule severely constrain its practical utilization. Furthermore, the generation of EtOH from CO_2 hydrogenation is much more difficult than methanol synthesis because of the subsequent carbon chain growth process being involved in EtOH formation. From the practical standpoint, the hydrogenation of CO_2 to EtOH is still poor and requires further development to find suitable and efficient catalyst.

In spite of the tremendous efforts devoted to EtOH synthesis via CO_2 hydrogenation using homogeneous catalysts [10–12], the use of the indispensable and air-sensitive organic ligands or additives limits their large-scale applications. Heterogeneous catalyst can overcome the drawbacks associated with organic complexes and shows more potential in industry. Many solid catalysts, such as Rh/SiO_2, $[Rh_{10}Se]/TiO_2$, CoMoS, physically mixed Fe- and Cu-based composite, and K/Cu-Zn-Fe have been used to efficiently synthesize EtOH from CO_2 hydrogenation [13–17], but most reactions are conducted at high temperatures (> 250 °C) and the low efficiencies need to be further improved. Han and co-workers have demonstrated an efficient Co_3O_4 supported Pt nanoparticles (NPs) catalyst (Pt/Co_3O_4) with excellent synergistic effect exhibited a good space-time-yield (STY) of alcohols, high selectivity to HAs, and robust stability on the reaction conditions of 200 °C and high total pressure of 8 MPa [18]. However, besides the inherent inconvenience accompanying with the handling problems, this catalytic process requires large amount of the indispensable solvent of complicated 1,3-dimethyl-2-imidazolidinone (DMI) [18]. Most recently, Huang et al. reported a highly ordered Pd–Cu NPs catalyst (Pd_2Cu/TiO_2) showing an unprecedented turnover frequency of 359 h^{-1} and high selectivity to EtOH (92%) at 200 °C and 3.2 MPa ($H_2/CO_2 = 3/1$) [19]. Therefore, development of an efficient heterogeneous catalyst system for EtOH synthesis from CO_2 hydrogenation (Scheme 1) without or with simple solvent under relatively mild conditions is urgently required.

Gold catalysts have been extensively used in past decades for many catalytic reactions [20–24]. It is also established that the small Au NPs can activate stable CO_2 and H_2 molecules and show excellent CO-tolerant ability [25]. During the search for a highly active and reusable catalyst for EtOH synthesis from CO_2 hydrogenation, we have recently found that a simple Au-based catalyst comprising of ultrasmall Au nanoclusters dispersed on anatase TiO_2 ($Au/a\text{-}TiO_2$) with abundant oxygen vacancies prepared by using deposition–precipitation (DP) method can achieve a high performance for EtOH generation under practical conditions (200 °C and 6 MPa) [26]. Although the parameters of catalyst preparation and the specific reaction conditions were systematically studied, the complicated preparation process consumed strong brønsted base and flammable H_2 gas which are not meet the principles of green chemistry [26]. Moreover, the time of the DP procedure was too long which can lead to the unnecessary waste of resources and energy.

Herein, we report an efficient photochemical method for the preparation of $Au/a\text{-}TiO_2$ catalyst for EtOH synthesis. Compared with the conventional DP method, the photochemical route is greener and more energy-saving and can spend shorter time for catalyst preparation. Given the well established fact that the preparation method strongly influences the performance of supported Au catalyst, the present work aims to identify the catalytic behavior of the $Au/a\text{-}TiO_2$

Scheme 1 EtOH synthesis from CO_2 hydrogenation. Compounds surrounded with dotted line are the possible products of primary HAs

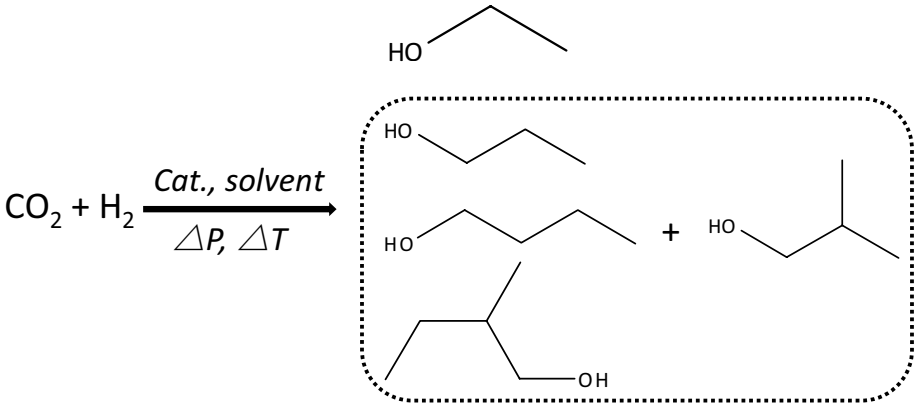

systems obtained by using photochemical route. To gain an insight into the respective nature of photo-stimulated Au/a-TiO_2 catalysts in relation to their performance in EtOH synthesis, extensive characterization by N_2 adsorption, X-ray diffraction (XRD), X-ray photoelectron spectroscopy (XPS), high-angle annular dark-filed scanning transmission electron microscopy (HAADF-STEM), UV–Vis diffuse reflectance (UV–Vis DR), and diffuse reflectance infrared Fourier transform (DRIFT) has been carried out.

2 Experimental

2.1 Catalyst Preparation

All chemicals were supplied by Aladdin and used without further purification. Anatase TiO_2 (a-TiO_2) was prepared using a hydrothermal method [27] with titanium bis (ammonium lactate) dihydroxide aqueous solution (TALH, 50%) and urea (99%). Typically, 10 mL TALH and 90 mL 0.1 M urea were mixed under stirring at room temperature. The resultant solution was then transferred into a Teflon-lined stainless autoclave, which was sealed and placed in an electric oven held at 160 °C for 24 h. The precipitate was separated by filtration and washed thoroughly with distilled water. After freeze-drying, the solid was obtained and calcined in air at 400 °C for 3 h with a ramp of 2 °C min^{-1}.

A photochemical procedure [28] was employed to prepare the Au/a-TiO_2 samples by illuminating for different times with a 300 W Xe lamp (Aulight CEL-HX, Beijing) and the power of the light source is calibrated to AM 1.5 by a NREL-calibrated Si cell (Oriel 91,150). Briefly, 0.5 g a-TiO_2 powder was dispersed in 200 mL distilled water and a certain amount of $HAuCl_4$ (e.g., 0.25 mM) was added to the suspension. After stirring at room temperature for 3 h, the photodeposition was performed under light irradiation for 5 s to 30 min. The Au/a-TiO_2 catalyst was separated by filtration, washed several times with distilled water, and freeze-dried completely. Once the mixed solution of 150 mL distilled water and 50 mL ethanol was used instead of sole distilled water, the finally obtained gold catalyst was denoted as Au/a-TiO_2(E).

2.2 Catalyst Characterization

The Brunauer–Emmett–Teller (BET) surface areas of the prepared catalysts were determined by adsorption–desorption of nitrogen at − 196 °C, using a Micromeritics TriStar 3000 equipment. Sample degassing was carried out at 300 °C prior to acquiring the adsorption isotherm. The metal loadings of the catalysts were measured by inductively coupled plasma atomic emission spectroscopy (ICP-AES) using iCAP 6300 spectrometer. XRD information of the samples was carried out on a German Bruker D8 Advance X-ray diffractometer using nickel filtered Cu Kα radiation at 40 kV and 40 mA. XPS data were recorded with a Perkin Elmer PHI 5000C system equipped with a hemispherical electron energy analyzer. The spectrometer was operated at 15 kV and 20 mA, and a magnesium anode (Mg Kα, $h\nu = 1253.6$ eV) was used. The

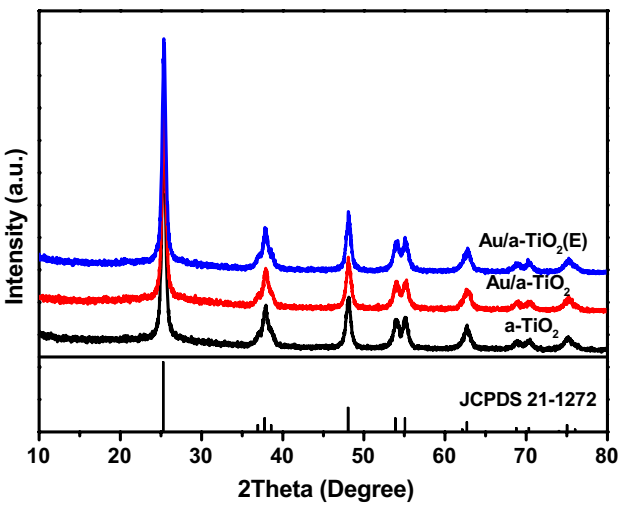

Fig. 1 XRD patterns of a-TiO_2, Au/a-TiO_2, and Au/a-TiO_2(E) catalysts

C 1s line (284.6 eV) was used as the reference to calibrate the binding energies (BE). HAADF-STEM images were obtained on a JEM 2100F electron microscope operating at 200 kV equipped with a field-emission-gun (FEG) and using an energy dispersive X-ray (EDX) unit (Si(Li) detector) and a HAADF detector. The samples for electron microscopy were prepared by grinding and subsequent dispersing the powder in ethanol and applying a drop of very dilute suspension on carbon-coated grids. The size distribution of the metal NPs was determined by measuring about 200 random particles on the images. The dispersion (D) of Au NPs can be estimated according to the relationship between the D and particle size as the following Eq. (1) [23, 29, 30], where d means the average size of Au NPs.

$$\mathrm{D}\,(\%) = \frac{1.0\ (\mathrm{nm})}{\mathrm{d}\ (\mathrm{nm})} \times 100\% \quad (1)$$

UV–Vis DR spectra of the solids diluted in $BaSO_4$ were recorded at room temperature on a Shimadzu UV 2401PC Spectrometer equipped with an integrating sphere and using $BaSO_4$ as reference. The DRIFT experiments were carried out on a Thermo Nicolet 6700 instrument equipped with a MCT detector and Harrick diffuse reflectance accessory. Spectra were obtained on the apparatus loaded with 50 mg of catalyst. Prior to the DRIFT test, sample was subjected to the pretreatment with Helium flow at 200 °C for removing any other gases and moisture. Each spectrum was obtained in Helium flow at room temperature and by subtracting the background (base spectrum) of the unpretreated sample.

2.3 Catalytic Activity Test

The experiments were carried out in high-pressure stainless autoclave reactor (Parr Instrument Co., 4790, 50 mL).

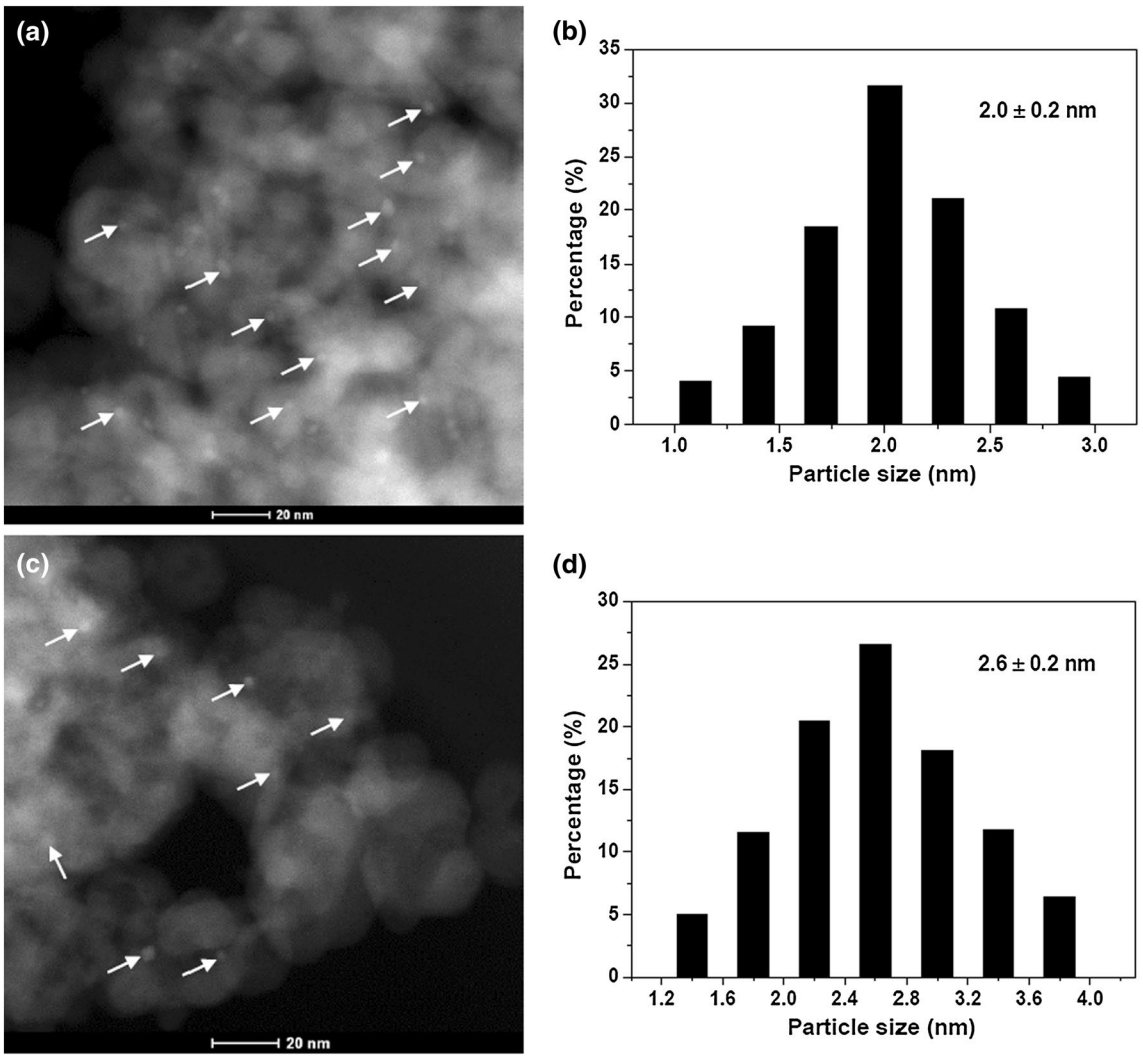

Fig. 2 HAADF-STEM images and Au particle size distributions of **a, b** Au/a-TiO_2 and **c, d** Au/a-TiO_2(E). The selected Au NPs are marked with arrows in (**a**) and (**c**)

Typically, 5 mL solvent of *N,N*-dimethylformamide (DMF) and a known amount of catalyst were placed in the autoclave. The autoclave was sealed and flushed many times with 0.5 MPa CO_2 to remove the air in the reactor, then CO_2 and H_2 gaseous mixtures were charged. The stirrer (800 rpm) was started until the desired temperature was reached. After a certain time, the autoclave was placed in cool water and the gas was carefully released. The gaseous mixture was analyzed using a gas chromatograph Agilent 7820A equipped with a TDX-01 column connected to a thermal conductivity detector. A known amount of internal standard 1,4-dioxane was added into the aqueous product in autoclave. The reaction mixture was transferred into a centrifuge tube and the solid catalyst was separated by centrifugation. The product solution was quantitatively analyzed using a gas chromatograph Agilent 7820A equipped with a HP-5 capillary column connected to a flame ionization detector. Identification of the products was performed by using a GC-MS spectrometer. For all the experimental data, the total carbon balance was > 95% and the experiments were repeated for three times to ensure the repeatability of the results. For the catalyst recycling experiment, the centrifuged catalysts were collected and washed with distilled water several times, followed by freeze-drying. The STY and selectivity to EtOH were calculated using Eqs. (2–5):

$$\text{STY (mmol g}^{-1}\text{ h}^{-1}) = \frac{\text{Generated EtOH (mmol)}}{\text{Total Au mass (g)} \times \text{time (h)}} \quad (2)$$

$$\text{STYsurface (mmol g}^{-1}\text{ h}^{-1}) = \frac{\text{Generated EtOH (mmol)}}{\text{Surface Au mass (g)} \times \text{time (h)}} \quad (3)$$

$$\text{Surface Au mass (g)} = \text{Total Au mass (g)} \times \text{D (\%)} \quad (4)$$

$$\text{SEtOH} = \frac{\text{Generated EtOH (mmol)}}{\text{Generated products (mmol)}} \times 100\% \quad (5)$$

3 Results and Discussion

3.1 Structural Characterization and Surface Properties

The a-TiO_2 material with abundant oxygen vacancies and noticeable specific surface area of 65 $m^2\ g^{-1}$ (Fig. S1) is favourable for the dispersion of the active Au NPs [26]. At the start of this work, we prepared the Au/a-TiO_2 and Au/a-TiO_2(E) with the actual Au loading of 0.3 wt% using photochemical method on light irradiation for 3 min. The well-defined crystal of anatase phase and the structure of supported gold catalysts are determined by XRD, and the corresponding results are shown in Fig. 1. a-TiO_2 exhibits a series characteristic diffraction peaks at 25.3°, 37.9°,

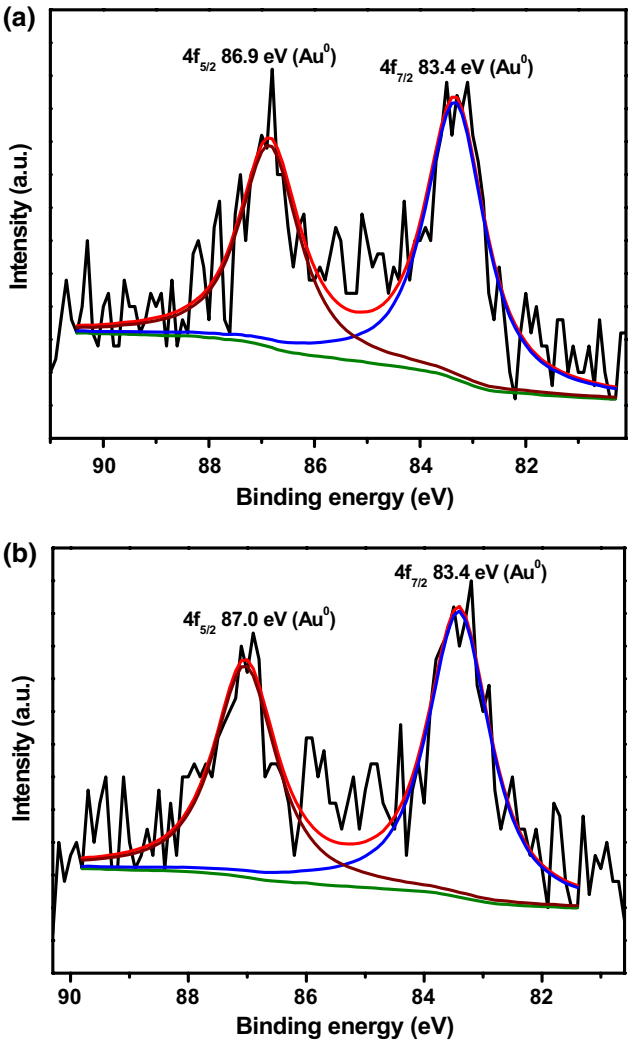

Fig. 3 XPS data of **a** Au/a-TiO_2 and **b** Au/a-TiO_2(E) catalysts

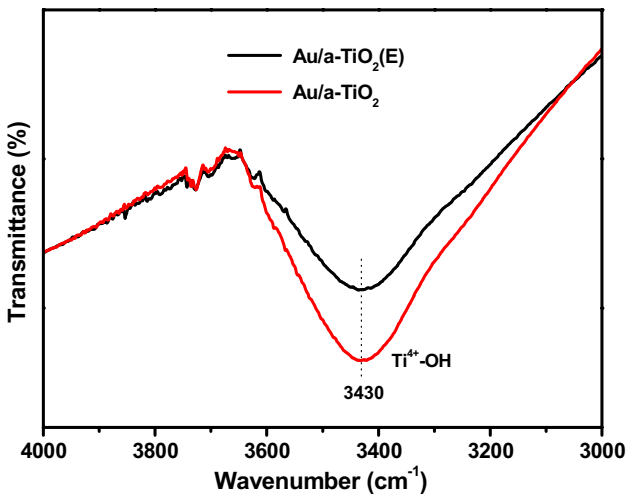

Fig. 4 DRIFT spectra of Au/a-TiO_2 and Au/a-TiO_2(E) catalysts

48.1°, 53.9°, 55.1°, and 62.7°, which are assigned to anatase phase (JCPDS 21-1272) [31]. It can be seen from Fig. 1 that the XRD patterns of these supported Au catalysts are very similar with a-TiO_2 material. There are no visible changes on structure after Au loading, and the absence of any Au-containing phases indicates the low Au loading and high dispersion of the Au species.

HAADF-STEM images in Fig. 2 and STEM-EDS mappings in Fig. S2 show that the Au NPs have been formed and homogeneously anchored on the a-TiO_2 surface. And the catalyst made in the solvent of water possesses slightly smaller Au NPs than that in the mixed solvent of EtOH-water system (2.0 vs. 2.6 nm). Meanwhile, the binding energies of ca. 87.0 eV for Au $4f_{5/2}$ and 83.4 eV for Au $4f_{7/2}$ clearly demonstrate that there is exclusive metallic gold on the surface of Au/a-TiO_2 and Au/a-TiO_2(E) samples (Fig. 3) [32]. Furthermore, the DRIFT band of 3430 cm^{-1}, as depicted in Fig. 4, assigned to the stretching vibration of H-bound OH groups in Ti^{4+}–OH (oxygen defects) indicates that Au/a-TiO_2 exhibits more oxygen vacancies than Au/a-TiO_2(E) and thus shows stronger metal-support interactions in Au–a-TiO_2 interface [26]. It is widely demonstrated that the defects like oxygen vacancies can act as reactive perimeter sites at the solid–solid interface (e.g., Au–a-TiO_2), and they can also in turn provide numerous highly mobile oxygen-containing species being able to react with CO_2 [33, 34].

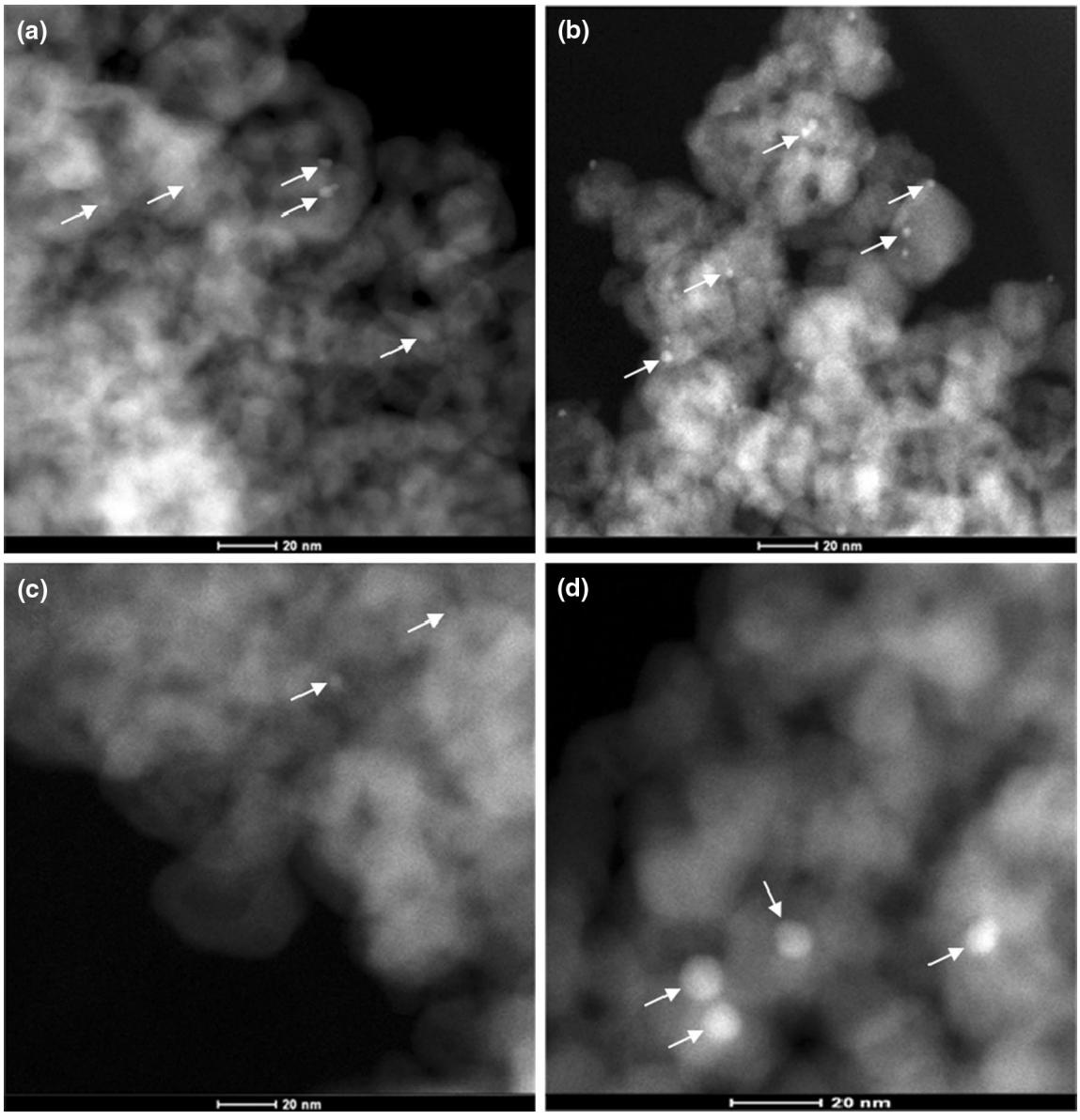

Fig. 5 HAADF-STEM images of Au/a-TiO_2 catalysts prepared on the irradiation time of **a** 5 s, **b** 1 min, **c** 10 min, and **d** 30 min. The selected Au NPs are marked with arrows

To further explore the effect of light irradiation and solvent on supported gold catalyst, we prepared the series of Au/a-TiO_2 and Au/a-TiO_2(E) samples by changing the irradiation time ranging from 5 s to 30 min. Irradiation time shows no visible effects on structure of gold catalysts (Fig. S3), but can significantly affect the Au particle size, as shown in Figs. 5 and 6. At the initial period of 5 s to 1 min, many small nuclei generated, and then aggregated to form Au NPs. Particle size of Au/a-TiO_2 is smaller than Au/a-TiO_2(E) in the irradiation time of within 3 min. When the irradiation time was prolonged further, the particles with larger diameters were obtained, for example 8.6 and 7.2 nm at the irradiation time of 30 min for Au/a-TiO_2 and Au/a-TiO_2(E), respectively. The UV–Vis spectra in Fig. 7 clearly show the apparent absorption peaks around 540 nm in the visible region for Au/a-TiO_2 and Au/a-TiO_2(E) catalysts due to the surface plasmon resonance of Au NPs [35]. The loading of Au NPs can also affect the shape of absorption peak remarkably. For Au/a-TiO_2 samples, the peak width increases with irradiation time > 3 min, probably due to the larger diameter of Au NPs. However, the peak width of Au/a-TiO_2(E) catalysts is insensitive to the prolongation of irradiation time. EtOH as a solvent is beneficial for the transfer of photogenerated electrons [36], which can induce the formation of Au NPs in shorter time (< 1 min) relative to that in sole water during preparation process. Furthermore, numerous

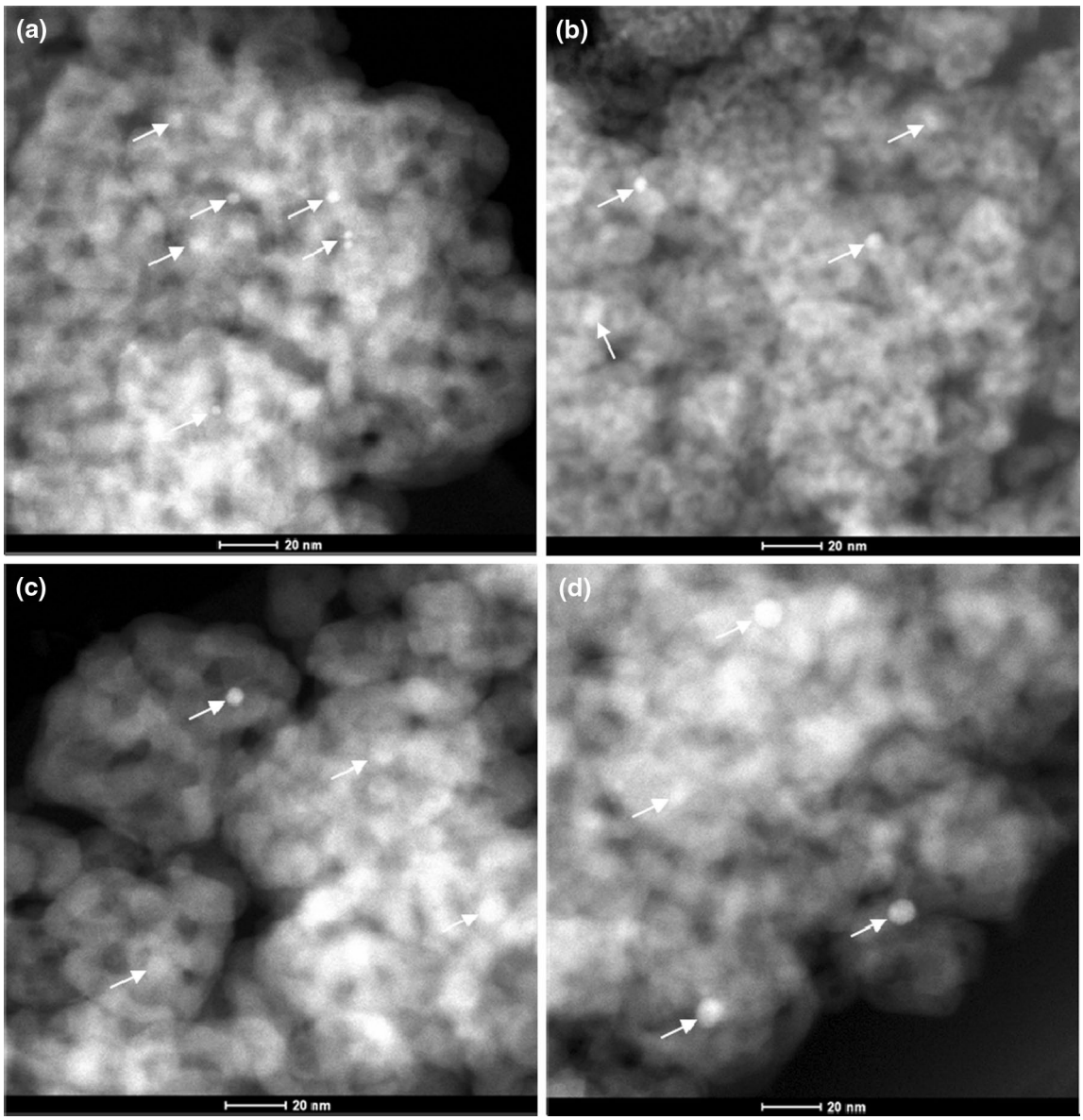

Fig. 6 HAADF-STEM images of Au/a-TiO_2(E) catalysts prepared on the irradiation time of **a** 5 s, **b** 1 min, **c** 10 min, and **d** 30 min. The selected Au NPs are marked with arrows

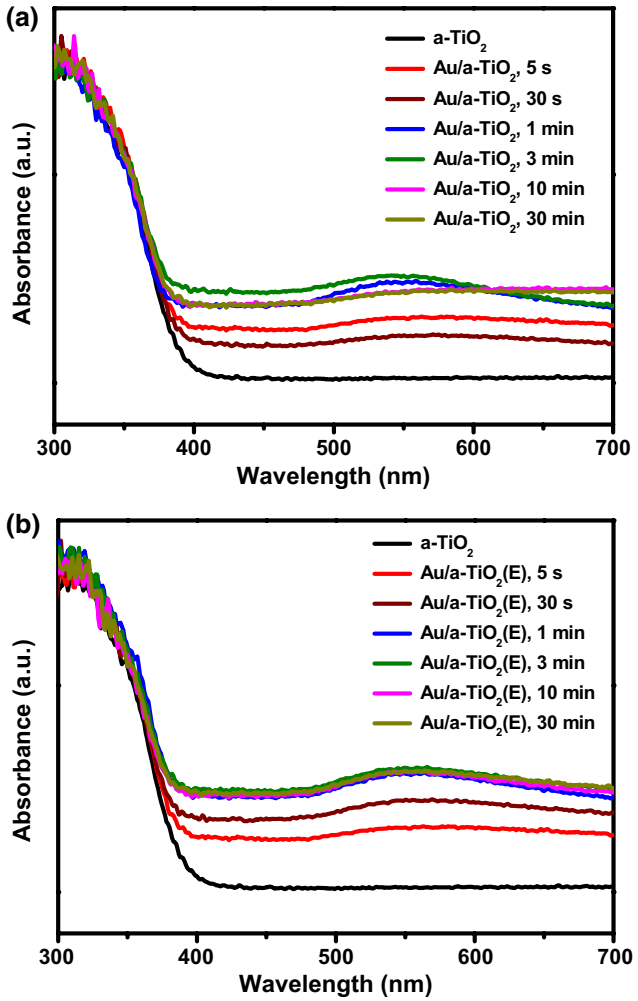

Fig. 7 UV–Vis spectra of **a** Au/a-TiO_2 and **b** Au/a-TiO_2(E) prepared on different irradiation time

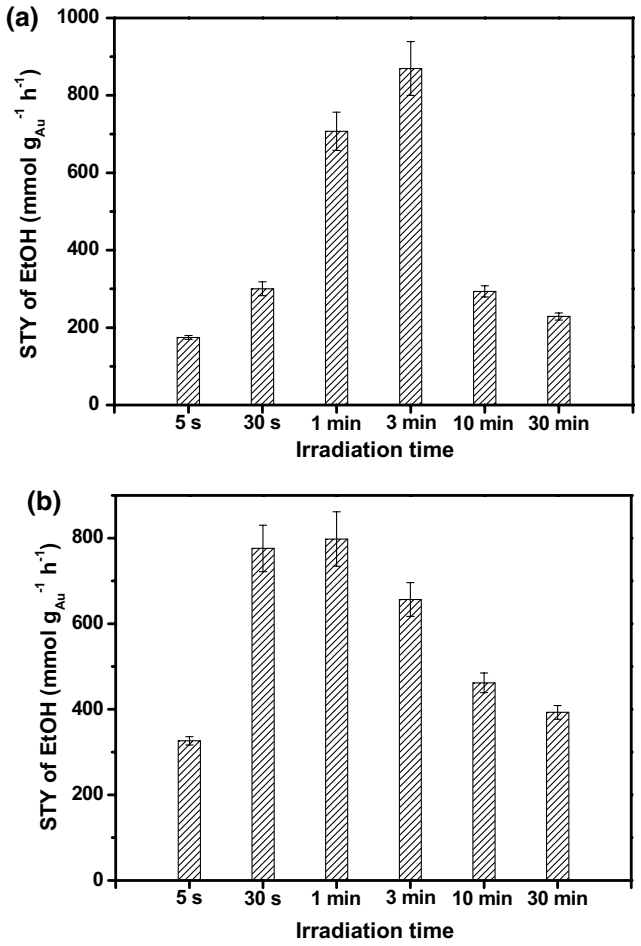

Fig. 8 Catalytic activities of **a** Au/a-TiO_2 and **b** Au/a-TiO_2(E) prepared on different irradiation time. Reaction conditions: 100 mg catalyst, 5 mL DMF, 45 bar H_2 and 15 bar CO_2 at 25 °C, 200 °C, 10 h. The standard deviation error bars are shown

dissolved oxygen in EtOH solution can consume the photogenerated electrons with the irradiation time of more than 3 min, thus preventing the accumulation of the electrons and the subsequent growth of Au NPs [37].

3.2 Catalytic Hydrogenation of CO_2 for EtOH Synthesis

The catalytic properties of the Au/a-TiO_2 and Au/a-TiO_2(E) catalysts prepared on different irradiation time for EtOH synthesis from CO_2 hydrogenation were evaluated on the optimal conditions of 45 bar H_2 and 15 bar CO_2 in DMF at 200 °C, which were demonstrated in our previous work [26]. With the irradiation time increasing, Au/a-TiO_2 catalyst exhibits the enhanced activities and achieves the highest STY of 869.3 mmol g_{Au}^{-1} h^{-1} at 3 min, as shown in Fig. 8a; however, the prolonged irradiation time of 10–30 min are found to give a negative effect on hydrogenation kinetics

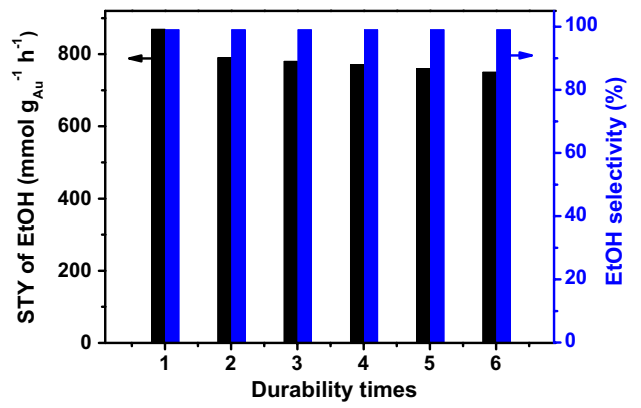

Fig. 9 Recycling of Au/a-TiO_2 catalyst for EtOH synthesis from CO_2 hydrogenation. Reaction conditions: 100 mg catalyst, 5 mL DMF, 45 bar H_2 and 15 bar CO_2 at 25 °C, 200 °C, 10 h

mainly due to the increased Au NPs. Noted that the maximum activity is comparable with the best ever-reported results for EtOH synthesis from CO_2 hydrogenation on the identical conditions [18, 19, 26]. The Au/a-TiO_2 catalysts also show excellent selectivity to the target product of EtOH (> 99%). The intrinsically electronic/geometric structure of Au NPs, suitable surface acid-base properties of a-TiO_2 support, and the strong Au–a-TiO_2 interactions endow the Au/a-TiO_2 catalyst with thermal catalytic functions of high activity and exceptional EtOH selectivity. On the other hand, Au/a-TiO_2(E) catalysts present the similar tendency as Au/a-TiO_2 on hydrogenation activity, but with the highest rate of 797.8 mmol g_{Au}^{-1} h^{-1} at the irradiation time of 1 min, as depicted in Fig. 8b. The increased Au NPs in Au/a-TiO_2(E) can also lead to the reduced performance. Compared with Au/a-TiO_2(E), the Au/a-TiO_2 catalysts show slightly higher performance for EtOH synthesis (e.g., the STYs of the catalysts prepared on the irradiation time of 3 min) attributed to the stronger metal-support interactions in Au/a-TiO_2 sample, which are consistent well with the DRIFT results demonstrated in Fig. 4. The possible reaction pathway for EtOH synthesis via CO_2 hydrogenation over Au/a-TiO_2 solid was proposed, as shown in Scheme S1. In the process of EtOH generation, the CO_2 was firstly hydrogenated to $–CH_3$ species, and then followed by CO insertion to form the intermediates of $–CH_3CO$, which were further hydrogenated into ethanol and subsequently desorbed from the catalyst surface [13, 17, 18, 26].

Having established that Au/a-TiO_2 as a reliable and efficient catalyst for EtOH synthesis from CO_2 hydrogenation under relatively mild conditions, we further investigated the reusability of the Au catalyst. As shown in Fig. 9, Au/a-TiO_2 is recoverable by simple treatment and proven robust even after six reuses. Noteworthy, the STY of EtOH generation in the 2nd run is only slightly lower than the fresh catalyst in the 1st run and keeps constant in the later recycling. Moreover, there is no significant loss of the selectivity to the target EtOH in the whole recycling experiments. Au/a-TiO_2 catalyst was removed from the reaction system after 5 h. Further processing of the filtrate on the reaction conditions for another 5 h did not result in any conversion. In addition, ICP-AES analysis of the filtrate indicates the content of Au or Ti leached is below the detection limit. These data confirm that the Au-catalyzed hydrogenation reaction occurs on the solid surface and the heterogeneous catalysis nature of Au/a-TiO_2 catalyst. Besides Au/a-TiO_2, the Au/a-TiO_2(E) catalyst also exhibits excellent stability (Fig. S4). Compared with the fresh catalysts, there is no significant change on morphology and no aggregation of Au NPs for the used counterparts (Figs. S5 and S6). These results suggest that a-TiO_2 supported Au NPs are very robust for EtOH synthesis from CO_2 hydrogenation.

3.3 Effect of Au Loading on EtOH Synthesis

It is well known that the size of Au NPs can significantly affect their catalytic behaviors in many reactions [23, 38, 39]. It was found that the size of Au NPs in Au/a-TiO_2 catalysts could be easily regulated by changing the concentration of the Au precursor from 0.05 to 0.25 mM with the deposition efficiency of 75–80% and/or the Au loading in the range of 0.3 to 1.5 wt% using photochemical method on irradiation time of 3 min. The initial $HAuCl_4$ solution with higher concentration or higher Au amount in the solution can accelerate the adsorption of Au-containing species on the underlying a-TiO_2 support during the stirring and subsequently improve the surface density of Au atoms in the preparation process [38]. The larger Au NPs can be formed with instaneous nucleation and continuous growth due to the accumulation of Au atoms. There are no visible changes on the structure with Au loading, as shown in Fig. 10, and the absence of any Au-containing phases suggests the high dispersion of the Au species even in high loadings. The particle size of Au/a-TiO_2 catalysts increases from 2.0 ± 0.2 to 6.9 ± 0.4 nm with the Au loading of 0.3 to 1.5 wt% (Figs. 2a, 11; Table 1).

Table 1 lists the effect of Au loading on the particle size of Au/a-TiO_2 catalyst and further on the activity for EtOH synthesis. It can be seen that the higher loading of gold element, the larger size of the Au NPs. With the increase of Au NPs, the Au/a-TiO_2 catalyst exhibits decreased performance for EtOH synthesis markedly from the STY of 869.3 mmol g_{Au}^{-1} h^{-1} for 2.0 ± 0.2 nm (0.3 wt%) to 393.4 mmol g_{Au}^{-1} h^{-1} for 4.7 ± 0.3 nm (1.2 wt%), as demonstrated in Table 1 and Fig. 12. The catalytic ability of 6.9 ± 0.4 nm Au NPs with loading of 1.5 wt% supported on a-TiO_2 is the lowest, showing the STY of only 272.8 mmol g_{Au}^{-1} h^{-1} on the identical

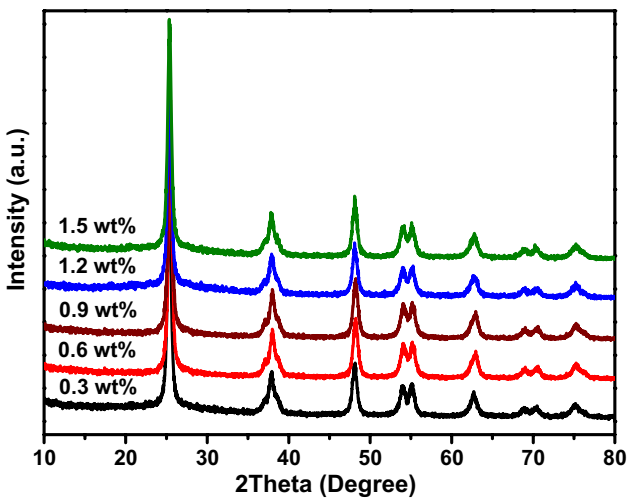

Fig. 10 XRD patterns of Au/a-TiO_2 catalysts with different Au loadings

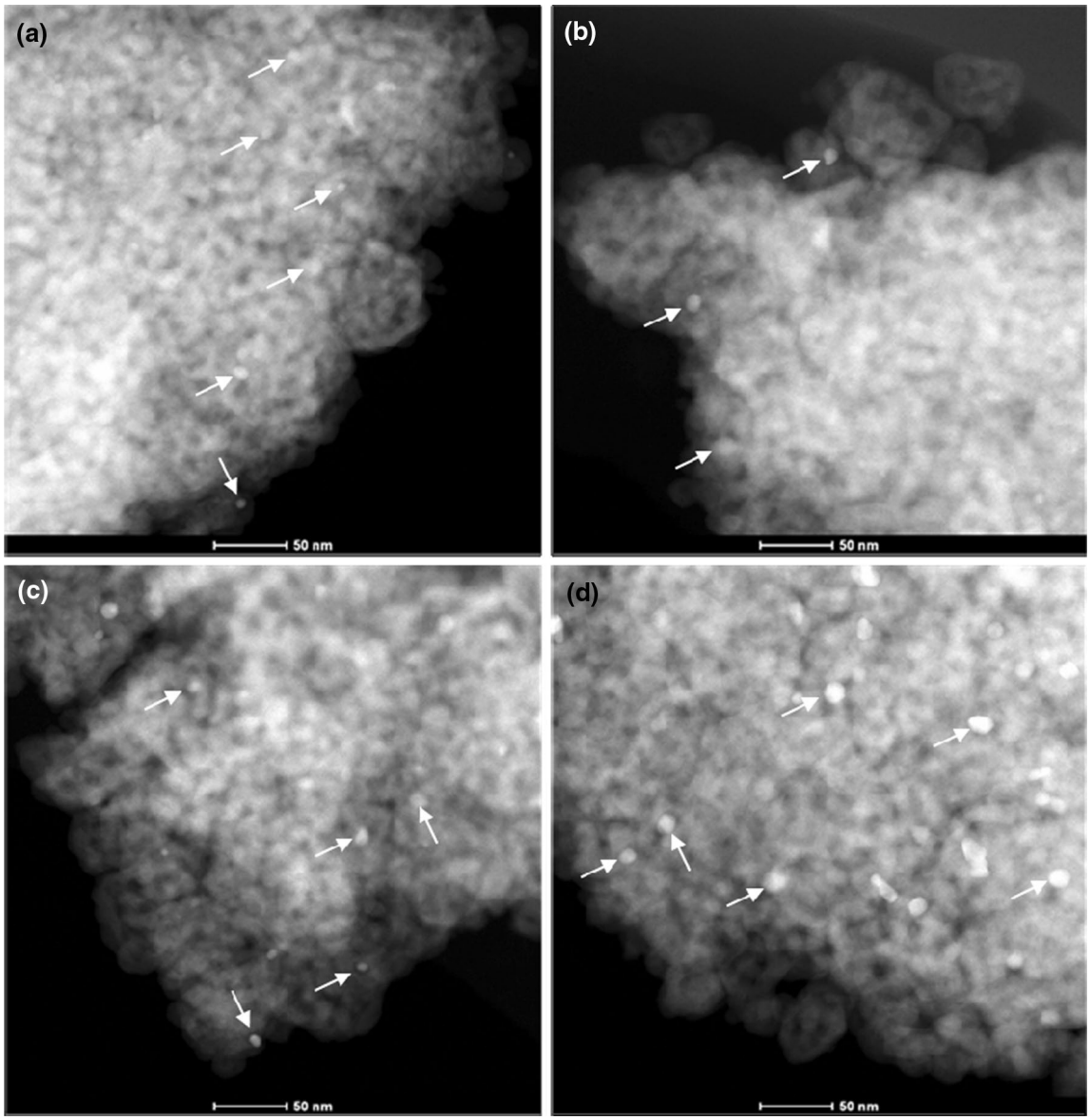

Fig. 11 HAADF-STEM images of Au/a-TiO_2 catalysts with Au loading of **a** 0.6, **b** 0.9, **c** 1.2, and **d** 1.5 wt%. The selected Au NPs are marked with arrows

conditions. Note that these Au catalysts show no significant loss on EtOH selectivity. Interestingly, there is an intrinsic consistency of the correlation on the Au loading or the size effect of Au NPs between hydrogenation performance and the surface gold active sites, as depicted in Fig. 12. The difference from the apparent activity of EtOH generation (STY) and the intrinsic activity ($STY_{surface}$) is ascribed to the different amount of active sites in calculation. It is widely accepted that the heterogeneous catalytic reactions are occurred on the surface or interface of solid samples and only surface metal species are the actual active sites [3, 23, 30]. The intrinsic activity in EtOH synthesis indicates the origin of gold catalysis in small molecule (e.g., CO_2) activation and transformation. These results suggest that the Au-catalyzed EtOH synthesis from CO_2 hydrogenation is a typical particle-size-dependent reaction.

4 Conclusions

We have demonstrated that an efficient anatase titania supported Au NPs catalyst was prepared using photochemical route for EtOH synthesis from CO_2 hydrogenation under relatively mind conditions. Compared with the conventional deposition–precipitation method requiring strong

Table 1 Effect of Au loading on Au/a-TiO_2 catalyst for EtOH synthesis

Entry	Au loading (wt%)[a]	Average size of Au NPs (nm)[b]	Dispersion (%)	STY (mmol g_{Au}^{-1} h^{-1})
1	0.3	2.0 ± 0.2	50.0	869.3
2	0.6	2.4 ± 0.2	41.7	751.4
3	0.9	2.9 ± 0.3	34.5	618.1
4	1.2	4.7 ± 0.3	21.3	393.4
5	1.5	6.9 ± 0.4	14.5	272.8

Reaction conditions 0.3 mg Au, 5 mL DMF, 45 bar H_2 and 15 bar CO_2 at 25 °C, 200 °C, 10 h

[a]The Au loading was determined by ICP-AES

[b]Determined from TEM

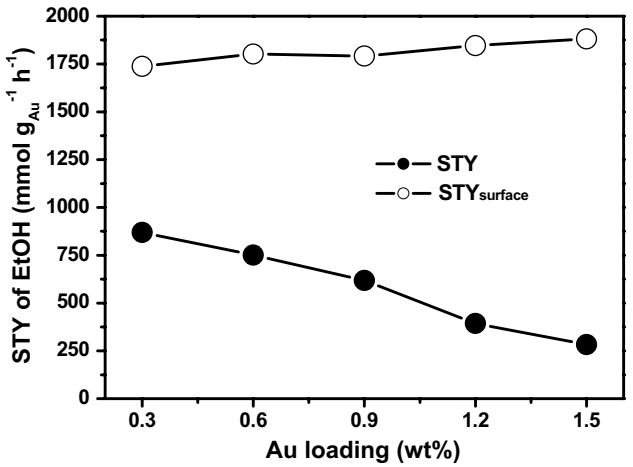

Fig. 12 Catalytic activity of Au/a-TiO_2 catalyst with different Au loading. Reaction conditions: 0.3 mg Au, 5 mL DMF, 45 bar H_2 and 15 bar CO_2 at 25 °C, 200 °C, 10 h

brønsted base and flammable H_2 gas in the complicated and time-consuming process, the photochemical way for the facile preparation of supported gold catalyst shows the unique advantages of green and energy-saving. The irradiation time, solvent, and metal loading are crucial for the catalytic properties. The engineered Au/a-TiO_2 with strong metal-support interactions and suitable Au loading exhibited outstanding activity and high selectivity to desired EtOH and showed excellent stability. The present findings can contribute to the design and preparation of more efficient metal based catalysts, especially on heterogeneous gold catalysis, using renewable solar energy for resource transformation in low-carbon energy supply system.

Acknowledgements This work was financially supported by the National Key Research and Development Program of China (2016YFB0901600), the NSF of China (61376056 and 51502331), and the STC of Shanghai (14520722000, 16ZR1440400, and 16JC1401700).

Compliance with Ethical Standards

Conflict of interest The authors declare that they have no conflict of interests.

References

1. Wang W, Wang S, Ma X, Gong J (2011) Chem Soc Rev 40:3703–3727
2. Aresta M, Dibenedetto A, Angelini A (2014) Chem Rev 114:1709–1742
3. Bi QY, Lin JD, Liu YM, He HY, Huang FQ, Cao Y (2016) Angew Chem Int Ed 55:11849–11853
4. Bi QY, Lin JD, Liu YM, Du XL, Wang JQ, He HY, Cao Y (2014) Angew Chem Int Ed 53:13583–13587
5. Goeppert A, Czaun M, Jones JP, Prakash GKS, Olah GA (2014) Chem Soc Rev 43:7995–8048
6. Luk HT, Mondelli C, Ferré DC, Stewart JA, Pérez-Ramírez J (2017) Chem Soc Rev 46:1358–1426
7. Sun X, Zhu Q, Kang X, Liu H, Qian Q, Zhang Z, Han B (2016) Angew Chem Int Ed 55:6771–6775
8. Spivey JJ, Egbebi A (2007) Chem Soc Rev 36:1514–1528
9. Sun D, Sato S, Ueda W, Primo A, Garcia H, Corma A (2016) Green Chem 18:2579–2597
10. Braunstein P, Matt D, Nobel D (1988) Chem Rev 88:747–764
11. Qian Q, Cui M, He Z, Wu C, Zhu Q, Zhang Z, Ma J, Yang G, Zhang J, Han B (2015) Chem Sci 6:5685–5689
12. Cui M, Qian Q, He Z, Zhang Z, Ma J, Wu T, Yang G, Han B (2016) Chem Sci 7:5200–5205
13. Kusama H, Okabe K, Sayama K, Arakawa H (1996) Catal Today 28:261–266
14. Nieskens DLS, Ferrari D, Liu Y, Jr RK (2011) Catal Commun 14:111–113
15. Kishida M, Yamada K, Nagata H, Wakabayashi K (1994) Chem Lett 23:555–556
16. Li S, Guo H, Luo C, Zhang H, Xiong L, Chen X, Ma L (2013) Catal Lett 143:345–355
17. Kieffer R, Fujiwara M, Udron L, Souma Y (1997) Catal Today 36:15–24
18. He Z, Qian Q, Ma J, Meng Q, Zhou H, Song J, Liu Z, Han B (2016) Angew Chem Int Ed 55:737–741
19. Bai S, Shao Q, Wang P, Dai Q, Wang X, Huang X (2017) J Am Chem Soc 139:6827–6830
20. Haruta M, Kobayashi T, Sano H, Yamada N (1987) Chem Lett 16:405–408
21. Johnston P, Carthey N, Hutchings GJ (2015) J Am Chem Soc 137:14548–14557
22. Wittstock A, Zielasek V, Biener J, Friend CM, Bäumer M (2010) Science 327:319–322
23. Bi QY, Du XL, Liu YM, Cao Y, He HY, Fan KN (2012) J Am Chem Soc 134:8926–8933
24. Liu X, He L, Liu YM, Cao Y (2014) Acc Chem Res 47:793–804
25. Preti D, Resta C, Squarcialupi S, Fachinetti G (2011) Angew Chem Int Ed 50:12551–12554
26. Wang D, Bi Q, Yin G, Zhao W, Huang F, Xie X, Jiang M (2016) Chem Commun 52:14226–14229
27. Liu L, Zhao H, Andino JM, Li Y (2012) ACS Catal 2:1817–1828
28. Oros-Ruiz S, Pedraza-Avella JA, Guzmán C, Quintana M, Moctezuma E, del Angel G, Gómez R, Pérez E (2011) Top Catal 54:519–526
29. Bond GC, Thompson DT (1999) Catal Rev Sci Eng 41:319–388

30. Tang H, Liu F, Wei J, Qiao B, Zhao K, Su Y, Jin C, Li L, Liu J, Wang J, Zhang T (2016) Angew Chem Int Ed 55:10606–10611
31. Yao X, Zhao R, Chen L, Du J, Tao C, Yang F, Dong L (2017) Appl Catal B 208:82–93
32. Bi QY, Lin JD, Liu YM, He HY, Huang FQ, Cao Y (2016) J Power Sources 328:463–471
33. Huang TJ, Lin HJ, Yu TC (2005) Catal Lett 105:239–247
34. Strunk J, Kähler K, Xia X, Comotti M, Schüth F, Reinecke T, Muhler M (2009) Appl Catal A 359:121–128
35. Yang S, Wang Y, Wang Q, Zhang R, Ding B (2007) Colloids Surf A 301:174–183
36. Hidalgo MC, Maicu M, Navío JA, Colón G (2009) J Phys Chem C 113:12840–12847
37. Kenens B, Chamtouri M, Aubert R, Miyakawa K, Hayasaka Y, Naiki H, Watanabe H, Inose T, Fujita Y, Lu G, Masuhara A, Uji-i H (2016) RSC Adv 6:97464–97468
38. Fang W, Chen J, Zhang Q, Deng W, Wang Y (2011) Chem Eur J 17:1247–1256
39. Liu SS, Liu X, Yu L, Liu YM, He HY, Cao Y (2014) Green Chem 16:4162–4169